Variability of the mesopause temperature and concentrations of reactive components of the mid-latitude atmosphere during sudden stratospheric warmings

Variability of the mesopause temperature and concentrations of reactive components of the mid-latitude atmosphere during sudden stratospheric warmings

I Medvedeva[1*], A Semenov[2]

[1]Institute of Solar-Terrestrial Physics, Siberian Branch of Russian Academy of Sciences, Irkutsk, 664033, Russia
[2]A.M. Obukhov Institute of Atmospheric Physics, Russian Academy of Sciences, Moscow, 119017, Russia

E-mail: ivmed@iszf.irk.ru

Abstract. We investigated the variations in the temperature regime, atomic oxygen, and ozone concentrations during the 2013 January major sudden stratospheric warming (SSW) and the 2017 February minor SSW. Data from the spectrometric observations of the hydroxyl emission at the longitudinally spaced mid-latitude sites Tory (51.8° N, 103.1° E) and Zvenigorod (55.7º N, 36.8º E), SABER TIMED satellite measurements and MERRA reanalysis were analysed. Concentrations of the atomic oxygen and ozone at the OH emission layer were calculated by using experimental data on the emission intensity and rotational temperature of the OH molecule, photochemical model of OH radiation, and MSISE-E-90 model. Significant changes in the OH temperature and emission intensity, as well as in the concentrations of atomic oxygen and ozone during the SSWs were revealed. These effects may be caused by variations in the height of the hydroxyl emission layer due to the enhancement of vertical motion in the atmosphere during the SSW. We found an increase in the day-to-day variability of the mesopause temperature up to 3 times in comparison with the mean seasonal values. This may indicate the SSW-associated intensification of the manifestation of the traveling planetary waves activity in the upper atmosphere.

1. Introduction

The temperature and dynamic regimes of the mesopause region feature great variability caused by the influence of atmospheric waves of different time scales, meteorological and climatic processes in the lower layers of the atmosphere, and solar radiation. One of the most significant meteorological disturbances, spreading to large spatial and temporal scales, is winter sudden stratospheric warming (SSW). SSW events, that occur in the winter hemisphere due to the interaction of planetary waves with a mean zonal flow, are the most obvious example of the coupling between different atmospheric layers. The SSW effect on the temperature, composition, and dynamics of the upper atmosphere is a subject of many experimental and theoretical studies. Thus, in [1], the authors reported significant ozone variations at the heights of the mesosphere and lower thermosphere (MLT) during the SSW events. Analyzing the 2009 January major SSW, the authors of [2] revealed a decrease in the atomic oxygen concentration during the SSW period and the [O] growth at the recovery phase. In [3] it was found, that the manifestation of the influence of sudden stratospheric warmings on the mesopause temperature depends on the region of observation and has a pronounced longitudinal effect. In [4, 5] the authors showed, that during SSW, the activity of atmospheric waves with different time scales increases.

In this paper, we present the results of studying the variations in the temperature, as well as in the atomic oxygen and ozone concentrations, during the 2013 major SSW and the 2017 January-February minor SSW. We analyzed the day-to-day temperature variability in the mesopause region during SSWs and compared the latter to the mean seasonal values. The analysis is based on the data of

measurements of the hydroxyl emission characteristics at the longitudinally spaced mid-latitude sites, Tory and Zvenigorod. Spectrometric observations of the airglow give information on the temperature and dynamics at the emission layers heights.

2. Data and analysis

Spectrometric measurements of the characteristics of the hydroxyl emission (band (6-2), 834.0 nm) are performed at the Geophysical Observatory of the Institute of Solar-Terrestrial Physics of the Siberian Branch of the Russian Academy of Sciences (51.8° N, 103.1° E, Tory), and at the Zvenigorod Station of the A.M. Obukhov Institute of Atmospheric Physics of the Russian Academy of Sciences (55.7° N, 36.8° E) in the patrol mode. Measurements and data processing at both observatories are implemented by uniform technique [6, 7, 8, 9]. Measurements are carried out at night time in the absence of strong clouds and full moon. To record the emission spectra of the upper atmosphere in the near-IR region, high-speed diffraction spectrographs equipped with highly sensitive digital receivers with CCD-cameras are used. A detailed description of the equipment and data processing technique is described in [6]. The spectra obtained with 10-minutes temporal resolution are used to determine the spectral characteristics (intensity, temperature) of the hydroxyl molecule emission arising at the mesopause region (the height of the OH emission maximum is ~ 87 km [8, 10]). The OH rotational temperature was derived by the distribution of the first three lines of the P-branch of the vibrational-rotational band OH(6-2), 834.0 nm. The method for determining the rotational temperature of the OH molecule was described in detail in [8, 11]. The accuracy of determining the OH rotational temperature by this technique is about 1-2 K. We analyzed data on the emission intensity and OH rotational temperature.
The rotational temperature of the OH molecule corresponds to the atmosphere temperature at the emission height. The hydroxyl emission intensity provides information on the concentration of reactive components at the OH emission layer heights.

To investigate the atmosphere temperature regime and variations in the OH emission maximum height in the analyzed regions, we used satellite data from the SABER TIMED, that measured the atmosphere temperature profiles and the Volume Emission Rate (VER) of the OH emission [12]. To estimate the OH emission layer height, OH VER profiles of the OH (1.6μm) were analyzed. We used the level 2A, version 2.0 SABER data obtained from the satellite night-time flybys over the investigated regions.

To estimate the temperature and dynamics of the middle atmosphere over the Northern Hemisphere, the MERRA (Modern ERA-Retrospective Analysis for Research and Applications) reanalysis daily data [13] were involved.

2.1. Calculation of the atomic oxygen and ozone concentrations in the mesopause region from the OH emission measurements

Hydroxyl emission results from recombination reactions of atomic oxygen produced in the atmosphere as a result of the molecular oxygen photodissociation, and is one of the channels of sink of the absorbed solar energy. The theory for producing excited OH molecules involves two basic mechanisms: ozone-hydrogen [14] and perhydroxyl [15]. Because the ozone-hydrogen mechanism is the main process of OH molecules excitation responsible for up to ~ 80% of the intensity of the total radiation, in this study, we used only the ozone-hydrogen mechanism.

This mechanism comprises a set of reactions:

$$O + O_2 + O_2 \rightarrow O_3 + O_2 \qquad \alpha_{O_3}(O_2)$$

$$O + O_2 + N_2 \rightarrow O_3 + N_2 \qquad \alpha_{O_3}(N_2)$$

$$H + O_3 \rightarrow OH(v \le 9) + O_2 \qquad \alpha_{HO_3}.$$

Vibrationally excited OH molecules ($v \le 9$) emit in the spectral region 0.5-5 μm [16] with an effective transition probability of

$$OH(v \le 9) \rightarrow OH + h\nu(0.5 \le \lambda \le 5\mu m) \qquad \bar{A} = 48\,s^{-1}$$

where Ā is the mean effective transition probability.

Based on the ozone-hydrogen mechanism for hydroxyl emission, using the recorded parameters of OH(6-2) emission and the known coefficients of reaction rates, it is possible to determine the concentration of atomic oxygen and ozone at the hydroxyl emission layer heights (80-100 km):

$$[O] = \frac{Q_{OH}(Z) \cdot \{A + k_{O_2} \cdot [O_2] + k_{N_2} \cdot [N_2]\}}{A \cdot \{\alpha_{O_3}(O_2) \cdot [O_2] + \alpha_{O_3}(N_2) \cdot [N_2]\} \cdot [O_2] \cdot B}, \left(cm^{-3}\right),$$

$$[O_3] = \frac{Q_{OH}(Z) \cdot \{A + k_{O_2} \cdot [O_2] + k_{N_2} \cdot [N_2]\}}{A \cdot \alpha_{HO_3} \cdot [H] \cdot B}, \left(cm^{-3}\right),$$

$$\text{where } B = 1 - \frac{Q_{OH}(Z) \cdot (k_O + k_d)}{A \cdot \{\alpha_{O_3}(O_2) \cdot [O_2] + \alpha_{O_3}(N_2) \cdot [N_2]\} \cdot [O_2]},$$

where α are the O_3 molecule production coefficients, k are the coefficients for the OH molecule deactivation by atoms and molecules. Here A is the (6-2) transition probability; the concentrations of the O_2, H and N_2 molecules are indicated in square brackets. Table 1 provides the values of the coefficients included in the formulas for [O] and [O_3] calculations. O_2, H and N_2 concentrations were calculated by using the MSIS-E-90 model.

Table 1. Coefficients used in the formulas above.

Coefficient		References
$\alpha_{O_3}(O_2) = 5.96\ 10^{-34}(300/T)^{2.37}$	$cm^6\,s^{-1}$	[17]
$\alpha_{O_3}(N_2) = 5.7\ 10^{-34}(300/T)^{2.62}$	$cm^6\,s^{-1}$	[17]
$\alpha_{HO_3} = 1.4\ 10^{-10}(480/T)$	$cm^3\,s^{-1}$	[18]
$\alpha_{HO_2} = 6.7\ 10^{-33}(238/T)$	$cm^6\,s^{-1}$	[19]
$\alpha_{OHO_2} = 2.9\ 10^{-11}(200/T)$	$cm^3\,s^{-1}$	[18]
$k_o = 5{,}00\ 10^{-11}$ см^3 с$^{-1}$	$cm^3\,s^{-1}$	[18]
$k_{O_2} = 1.05\ 10^{-11}\exp(220/T)$	$cm^3\,s^{-1}$	[20]
$k_{N_2} = 3.36\ 10^{-13}\exp(220/T)$	$cm^3\,s^{-1}$	[20]
$A = 0.91$	s^{-1}	[21]

2.2. Estimating the OH temperature variability

By using the technique described in [7, 22, 23] in detail, we analyzed the OH temperature variability during the 2013 and 2017 SSWs. As a parameter for the temperature variability, the OH rotational temperature standard deviations in the annual variations were used. To estimate the temperature day-to-day variability, the seasonal variations were excluded from the nightly averaged temperature sets. The seasonal variation harmonics were calculated by fitting (through the least square method) the nightly averaged temperature sets by the function:

$$T = \overline{T} + \sum_{n=1}^{3} A_n \cos(\frac{2\pi n}{365.25}(t_d - \varphi_n))$$

where $\overline{T}$ is the mean temperature; n is the harmonics number; A_n and φ_n are its amplitude and phase; t_d is the day of year.

Figure 1(a) shows the nightly mean temperature (dots) obtained at the Tory station in 2017 and average seasonal variations (solid lines) calculated by the sum of the first three harmonics. To determine the temperature day-to-day variability, seasonal variations were excluded from a set of its nightly values, and then the residual temperature deviations were analyzed (Figure 1(b)). Day-to-day variability in the mesopause temperature is mainly caused by influence of traveling planetary waves (PW), so, this method enables to analyze the PW activity at these altitudes.

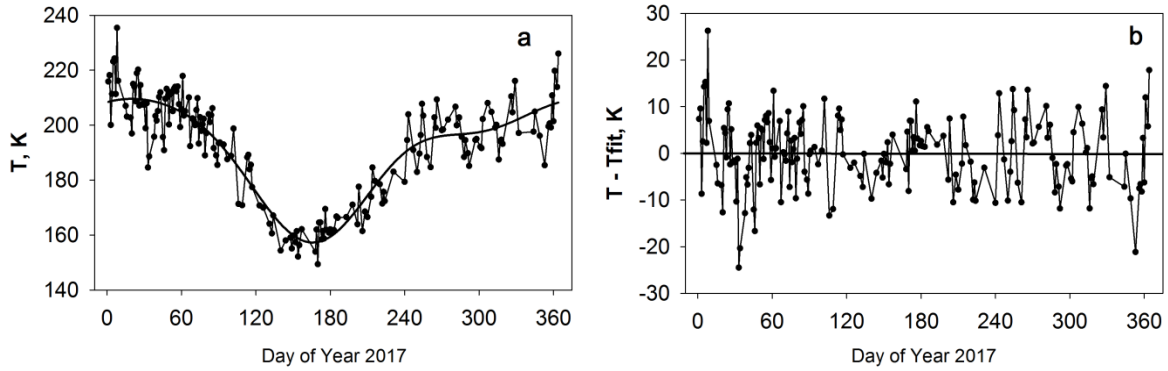

Figure 1. (a) - nightly mean values of the OH temperature (dots) obtained at the Tory station in 2017 and the seasonal variations (solid line) calculated by the sum of harmonics with periods of 12, 6 and 4 months. (b) - residual temperature deviations after subtraction of the seasonal variations.

After subtraction of the seasonal variations, relative residual deviations of the temperature normalized on mean temperature $|\Delta_{dd}|$ have been analyzed.

3. Results and discussion

3.1. Stratosphere temperature and dynamics in 2013 and 2017 winters

The 2013 January and 2017 January-February sudden stratospheric warmings caused significant disturbances in the zonal characteristics of the Northern Hemisphere stratosphere. To estimate the stratosphere disturbance, the MERRA data on the stratosphere zonal parameters for the 10 hPa pressure level were used.

Figure 2 shows variations in the stratosphere characteristics over the Northern hemisphere at the 10 hPa level (~32 km), obtained from the MERRA reanalysis data: zonal mean (60-90º N) temperature (a) and zonal mean zonal wind at 60º N (b), which is an indicator of the circumpolar vortex strength. The plots in the left panel of figure 2 correspond to the 1.12.2012-15.02.2013 time interval, those in the right panel – to 1.01.2017-15.03.2017.

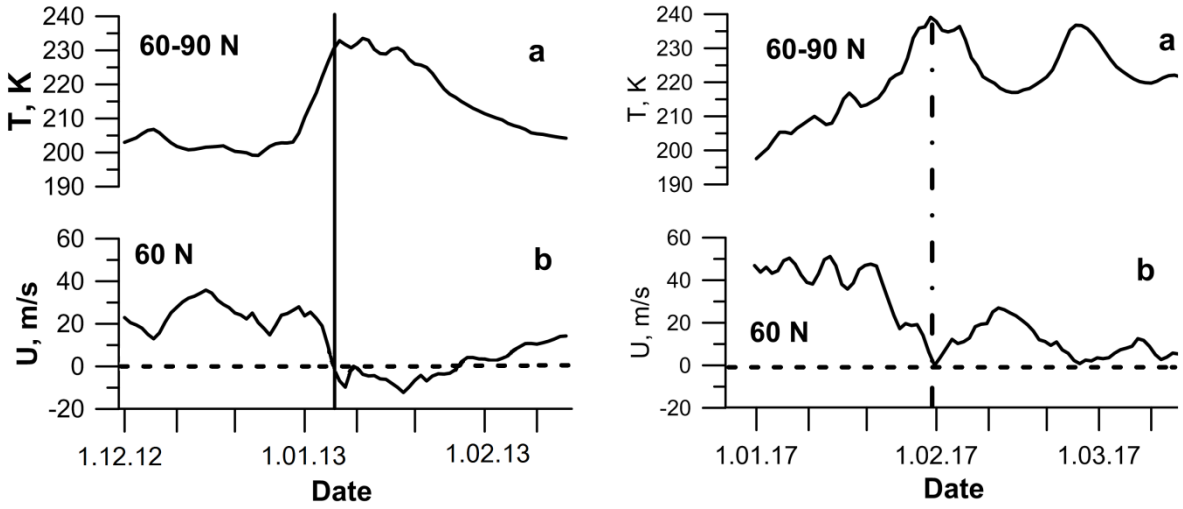

Figure 2. Zonal characteristics of the stratosphere at 10 hPa (~32 km), MERRA reanalysis data: (a) - zonal mean (60–90º N) temperature; (b) – zonal mean (60º N) zonal wind. The plots on the left panel correspond to the 1.12.2012-15.02.2013 time interval, those in the right panel – to 1.01.2017-15.03.2017. Vertical solid line (left) marks the zonal mean zonal wind reversal in January 2013. Vertical dashed-dotted line (right) marks the peak of the 2017 SSW.

According to the MERRA data, in 2013 early January, there were significant disturbances in the temperature and dynamic regimes of the middle atmosphere (the left panel of figure 2). The temperature of the stratosphere at high latitudes began to rise in late December, and, in early January, it increased by ~30 K and persisted high until the end of January (Figure 2(a)). The zonal mean zonal wind (60º N, 10 hPa) changed its direction from western to eastern on January 5-6 and remained so until ~ January 20 (Figure 2(b)). Thus, in January 2013, major SSW developed over the Northern hemisphere, it caused disturbances in the temperature and dynamic regime of the middle atmosphere over a wide range of latitudes. In late January and early February 2017, there were also significant perturbations of the state of the middle atmosphere over the Northern Hemisphere (right panel of figure 2): there were the temperature increase by ~40K (Figure 2(a)), weakening of the mean-zonal wind by ~ 50 m/s without reversal (Figure 2(b)). Thus, in January-February 2017 a minor SSW occurred.

3.2. Manifestations of the major 2013 and minor 2017 sudden stratospheric warmings in the mesopause region

3.2.1. 2013 January SSW

To study the atmosphere state over Tory and Zvenigorod sites, the SABER data on the temperature profiles for the 2012 December 1 - 2013 January 31 time interval were used. Figure 3 shows variations in the atmosphere temperature over the 15-100 km height range in the analyzed regions from the SABER data. Apparently, that from the end of December, significant disturbances in the temperature regime within a large range of the atmospheric heights have been observed in the investigated regions. Figure 3 also shows the variations in the night-averaged values of the OH temperature (b), day-to-day temperature variability (c), and the OH emission intensity (d), obtained from ground-based spectrometric observations at Tory (left) and Zvenigorod (right), as well as variations in the concentrations of ozone (e) and atomic oxygen (f), calculated through the procedure described above.

For the Tory site, at the height of the hydroxyl emission, the following effects were revealed (Figure 3, left panel). During the SSW evolution from late December, one observed the rise in the OH temperature (by ~15-20 K), OH emission intensity (by over a factor of 2), as well as in the ozone (by up to a factor of 2) and in the atomic oxygen (by up to a factor of 3) concentrations as compared with

the values observed prior to the SSW onset. Over January 2-4, T(OH), I(OH), [O_3] and [O] decreased, then, just after the moment of the zonal wind reversal and the major SSW onset, their values increased again. However, 5-7 days later, the T(OH), I(OH), [O_3] and [O] values recovered to the level observed in the SSW absence with a short-time increase during the recovery of the winter zonal circulation on January 20s. In mid-December, at the beginning of the SSW evolution, there were observed increased values of day-to-day OH temperature variability caused by the impact of traveling planetary waves (Figure 3(c)). The average values of day-to-day variability calculated from the Tory data over 2008-2015 for December and January are ~ 5% [23], whereas in 2012 December, its values reached 8-10%.

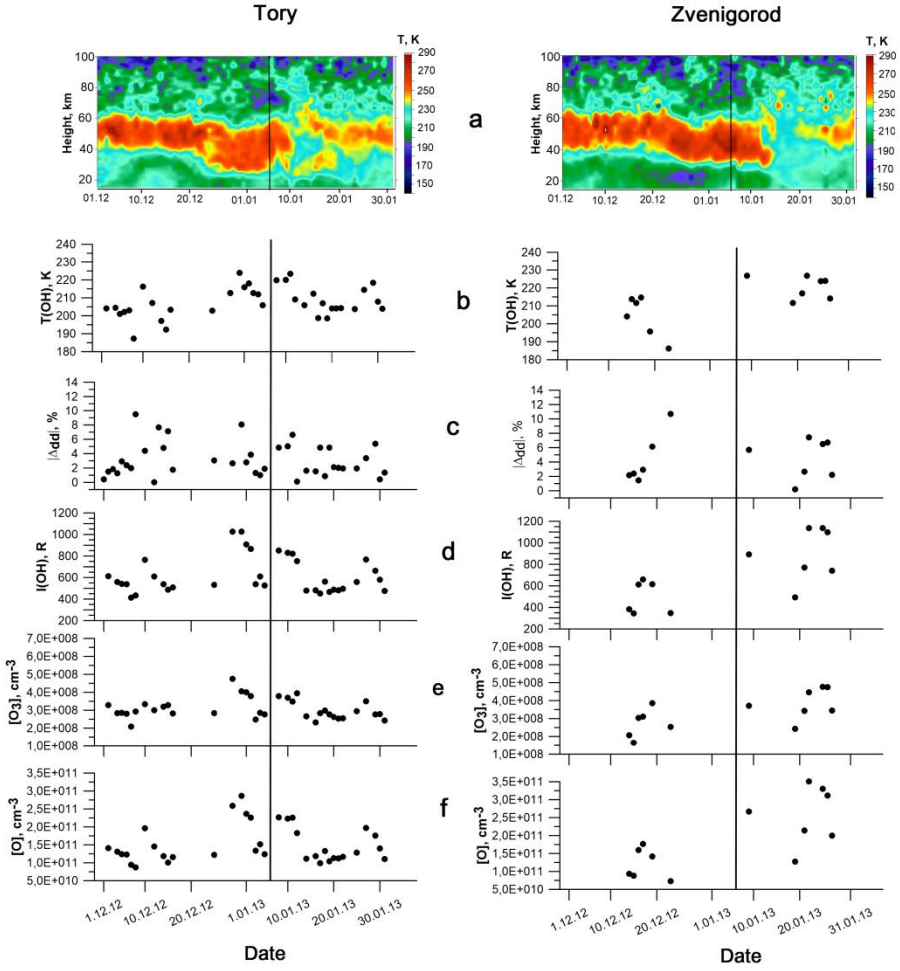

Figure 3. Day-to-day variations in: (a) - atmosphere temperature from the SABER data; (b) - OH rotational temperature (T(OH)); (c) - day-to-day OH temperature variability (|Δdd|); (d) - intensity of the OH emission (I(OH)); (e) - ozone concentration ([O_3]), (f) - atomic oxygen concentration ([O]). Left panel – for Tory site, right panel – for Zvenigorod site. [O] and [O_3] are calculated through the above procedure. Vertical line shows reverse of zonal mean zonal wind. The analyzed time interval is 2012 December 1 – 2013 January 31.

From the data of ground-based spectrometric observations in Zvenigorod (Figure 3, right panel), during the development of the SSW, a decrease in OH temperature by ~ 30 K (b) was observed. In this time interval, the value of day-to-day temperature variability reached ~11% (c), while the average variability values calculated for the period 2000-2011 for Zvenigorod are ~3.5% for December and January [2]. In contrast to the results obtained from Tory data, significant rise (by a factor of ~3) in the OH emission intensity, in the [O_3] (by a factor of ~ 2), and in the [O] (by a factor of ~3.5) relative to the values at the SSW onset occurred during the SSW recovery phase.

3.2.2. 2017 January-February SSW

Figure 4(a) presents height-temporal variations in the atmosphere temperature over the 15-100 km height range over Tory (left) and Zvenigorod (right) from the SABER data for 2017 January 1 - 2017 February 28. From these data, significant perturbations of the atmospheric temperature regime originated in late January and extended to large range of heights. The same figure also shows the variations in the night-averaged values of the OH temperature (b), day-to-day temperature variability (c), and the OH emission intensity (d), obtained from ground-based spectrometric observations at Tory (left) and Zvenigorod (right), as well as calculated variations in the concentrations of ozone (e) and atomic oxygen (f).

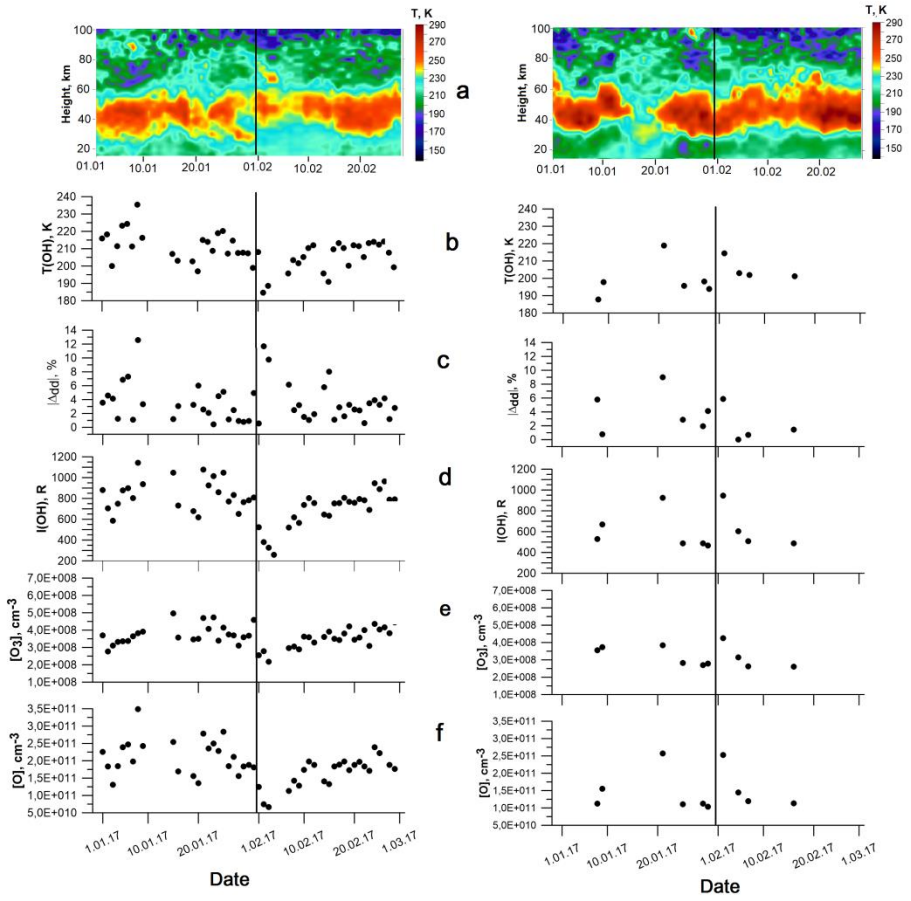

Figure 4. Day-to-day variations in: (a) - atmosphere temperature from the SABER data; (b) - OH rotational temperature (T(OH)); (c) - day-to-day OH temperature variability (|Δdd|); d - intensity of the OH emission (I(OH)); (e) - ozone concentration ([O_3]), (f) - atomic oxygen concentration ([O]). Left panel – for Tory, right panel – for Zvenigorod. [O] and [O_3] are calculated through the above procedure. Vertical line marks the SSW peak. The analyzed time interval is 2017 January 1 - 2017 March 1.

For the Tory site, at the height of the hydroxyl emission the following effects were found (Figure 4, left panel). In the first half of January, there was a significant increase in T (OH) by ~ 20-25 K (b); the growth in I (OH) by a factor of ~2 (d), [O_3] by a factor of ~1.5 (e) and [O] by a factor of ~2. However, already on January 31-February 1, when the zonal temperature of the stratosphere at 10 hPa reached its maximal value (~240 K), and the zonal wind weakened to almost 0 m/s (Figure 2), a significant cooling at the OH emission height occurred, the temperature dropped to ~185 K (b). At the same time, extremely low, up to ~250-300 R, values of the OH emission intensity were observed (d). The [O_3] decreased by a factor of ~2 (e) and [O] by a factor of ~3 relative to the values in early January. During

the 2017 SSW, day-to-day temperature variability reached 11-13%, while the average 2008-2015 values calculated from Tory data were ~5% for January and ~4% for February [23].

Unfortunately, because of bad weather conditions during this time interval, the data of spectrometric observations in Zvenigorod, suitable for analysis, are few. However, from these data, it is possibly to conclude that, in contrast to the results for the Tory site, there was no evident decrease in T (OH) (b); I (OH) (d), [O_3] (e), and [O] (f) around February 1. Analysis of day-to-day variability of the OH temperature during the SSW revealed its intensification by ~10%. Note, that the average 2000-2011 values of variability for Zvenigorod are ~3.5% for January and ~4.5% for February [7].

In [2, 24], it was shown, that the OH emission intensity increased at the decrease in the OH emission layer height. To find a possible cause for the revealed significant variations in T(OH), I (OH), [O], and [O_3] during the 2013 and 2017 SSWs, variations in the height of the OH emission layer have been analyzed. For this purpose, the data from SABER measurements of the Volume Emission Rate (VER) of the OH 1.6 μm emission were used. For each VER profile, the height of the emission maximum was determined. Figure 5 presents regression dependences between the OH emission intensity and the emission maximum height for the Tory (top panel) and Zvenigorod (bottom panel) sites. Left panels correspond to the 2013 SSW, the analyzed time interval is 2012 December 14 - 2013 January 31. Right panels are the same for the 2017 SSW, the analyzed time interval is 2017 January 1 - 2017 February 28.

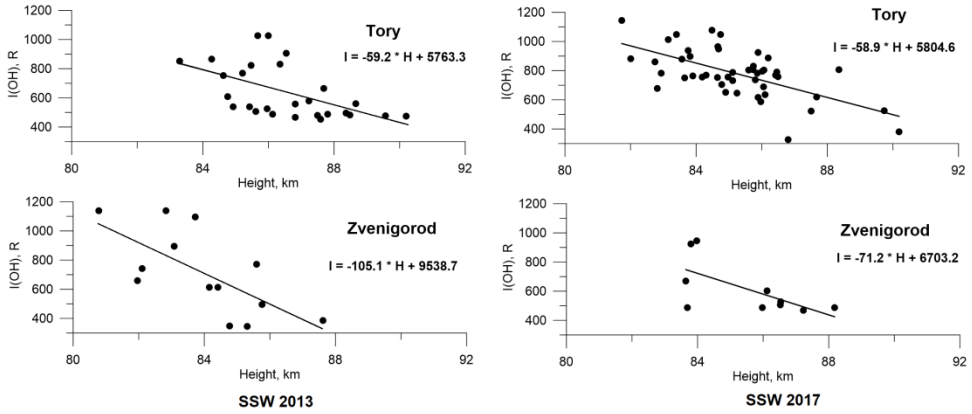

Figure 5. Regression dependences of the OH emission intensity on the emission layer maximum height for the Tory (top panel) and Zvenigorod (bottom panel) sites. Left panels correspond to SSW 2013, the analyzed time interval is 2012 December 14 - 2013 January 31. Right panels – for the 2017 SSW, the analyzed time interval is 2017 January 1 - 2017 February 28.

All the plots show a clear anticorrelation between the hydroxyl emission intensity and height. Over the analyzed 2013 SSW period, the OH emission maximum height varied from 83 km to 90 km for Tory and from 81 km to 88 km for Zvenigorod. During the 2017 SSW, the OH emission maximum height changed from 82 km to 90 km for Tory and from 84 km to 88 km for Zvenigorod.

Thus, the revealed significant variations in the OH emission intensity and temperature, as well as in the concentration of atomic oxygen and ozone in the mesopause region, may be due to a change in the height of the hydroxyl emission layer. Variations in the OH emission height, in turn, may be caused by enhancement of the vertical motion in the atmosphere during the SSWs period. An inverse dependence between the hydroxyl layer maximum height and the OH emission intensity was also revealed in [2, 24, 25].

The downward motion results in the OH emission layer decrease, which leads to its adiabatic heating. As a result, there is an increase in the OH temperature, of the atomic oxygen concentration, and, as a consequence, an increase in the OH emission intensity. Upward motion, on the contrary, results in increase in the OH emission layer height, which leads to an adiabatic cooling, to a decrease in the OH temperature, in the atomic oxygen concentration, and in the OH emission intensity. Similar

results and conclusions and a possible mechanism explaining the [O] variation with upward or downward motion in the atmosphere were presented and discussed in [2]. According to [2], downward motion results in an influx of atomic oxygen from the thermosphere, where its concentration is higher, than that in the mesopause region, to the OH emission heights. Upward motion brings air masses with a low [O] to the hydroxyl emission heights from the lower atmosphere [2].

The revealed longitudinal differences in the SSW effects in the mesopause region the for Tory and Zvenigorod sites can be caused by differences in the dynamics of the underlying atmosphere.

4. Conclusions

We studied the temperature regime and concentrations of reactive components of the atmosphere in the mesopause region during the 2013 January major SSW and the 2017 January-February minor SSW. The analysis is based on the ground-based spectrometric measurement data on the OH(6-2) hydroxyl emission at the Tory (51.8° N, 103.1° E) and Zvenigorod (55.7° N, 36.8° E) stations, with involving the SABER TIMED satellite measurements and MERRA reanalysis data. We also analyzed day-to-day mesopause temperature variability due to the impact of traveling planetary waves. Variations in the atomic oxygen and ozone concentrations in the mesopause region were calculated from the experimental data on the OH (6-2) temperature and emission intensity, by using the photochemical model of hydroxyl emission, and the MSIS-E-90 atmosphere model.

It is found, that SSW events can cause a significant changes in the OH temperature and emission intensity, as well as in the concentrations of atomic oxygen and ozone at the height of the OH emission. The revealed effects may be caused by variations in the hydroxyl emission layer height due to the enhancement of vertical motion in the atmosphere during the SSW.

During the analyzed sudden stratospheric warmings, the day-to-day variability of the mesopause temperature increased up to 3 times in comparison with the mean seasonal values. This may indicate an intensification of the manifestation of the activity of traveling planetary waves in the upper atmosphere during the SSW.

The observed longitudinal differences in the SSW effect manifestation in the mesopause region in the observed regions Tory and Zvenigorod may be caused by differences in the dynamics of the underlying atmosphere.

Acknowledgements

This study was financially supported by the Grant from the Russian Science Foundation (Project N 18-17-00042). The experimental data recorded by the equipment of Center for Common Use «Angara» http://ckp-rf.ru/ckp/3056/ at the ISTP SB RAS (Tory Station) obtained within the Basic Research program II.16 were used. We thank the SABER/TIMED team for the access to the temperature and emission rates data, and the MERRA team for the access to the reanalysis data.

5. References

[1] Tweedy O V, Limpasuvan V, Orsolini Y J, Smith A K, Garcia R R, Kinnison D, Randall C E, Kvissel O-K, Stordal F, Harvey L, Chandran A 2013 Nighttime secondary ozone layer during major stratospheric sudden warmings in specified-dynamics WACCM *J. Geophys. Res. Atmos.* **118** pp 1-13

[2] Shepherd M G, Cho Y M, Shepherd G G., Ward W, Drummond J R 2010 Mesospheric temperature and atomic oxygen response during the January 2009 major stratospheric warming *J. Geophys. Res.* **115** A07318

[3] Medvedeva I V, Semenov A I, Chernigovskaya M A, Perminov V I 2012 Studying Manifestations of 2008–2011 Sudden Stratospheric Warmings in East-Siberia and European Russia *Geophysica* **48(1-2)** pp 91-103

[4] Limpasuvan V, Richter J H, Orsolini Y J, Stordal F, Kvissel O-K 2012 The roles of planetary and gravity waves during a major stratospheric sudden warming as characterized in WACCM *Journal of Atmospheric and Solar-Terrestrial Physics* **78-79** pp 84-98

[5] Yigit E, Medvedev A S 2015 Internal wave coupling processes in Earth's atmosphere *Adv. Space Res.* **55** pp 983–1003

[6] Semenov A I, Bakanas V V, Perminov V I, Zheleznov Yu A, Khomich Yu V 2002 The near infrared spectrum of the emission of the nighttime upper atmosphere of the Earth *Geomagnetism and Aeronomy* **42(3)** pp 390-397.
[7] Perminov V I, Semenov A I, Medvedeva I V, Pertsev N N 2014 Temperature Variations in the Mesopause Region According to the Hydroxyl-Emission Observations at Midlatitudes *Geomagnetism and Aeronomy* **54(**2) pp 230-240
[8] Khomich V Yu, Semenov A I, Shefov N N 2008 Airglow as an Indicator of Upper Atmospheric Structure and Dynamics / Berlin Heidelberg: Springer-Verlag 740 p
[9] Medvedeva I V, Semenov A I, Perminov V I, Beletsky A B, Tatarnikov A V 2014 Comparison of Ground-based OH Temperature Data Measured at Irkutsk (52°N, 103°E) and Zvenigorod (56°N, 37°E) Stations with Aura MLS v3.3 *Acta Geophysica*. **62(2)** pp 340-349
[10] Baker D J, Stair A T 1988 Rocket measurements of the altitude distribution of the hydroxyl airglow *Physica Scripta* **37(4)** pp 611–622
[11] Shefov N N 1961 On determination of the rotational temperature of the OH bands. In: *Krassovsky, V.I. (ed) Spectral, electrophotometrical and radar researches of aurorae and airglow* **5** USSR Acad Sci Publ House pp 5–9
[12] Russell J M III, Mlynczak M G, Gordley L L, Tansock J, Esplin R 1999 An overview of the SABER experiment and preliminary calibration results *Proc. SPIE* **3756** pp 277–288
[13] Gelaro R, McCarty W, Suárez M J, Todling R, Molod A, Takacs L, Randles C A, Darmenov A, Bosilovich M G, Reichle R, Wargan K, Coy L, Cullather R, Draper C, Akella S, Buchard V, Conaty A, da Silva A M, Gu W, Kim G-K, Koster R, Lucchesi R, Merkova D, Nielsen J E, Partyka G, Pawson S, Putman W, Rienecker M, Schubert S D, Sienkiewicz M Zhao B 2017 The Modern-Era Retrospective Analysis for Research and Applications, Version 2 (MERRA-2) *J. Climate* **30(14)** pp 5419-5454
[14] Bates D R, Nicolet M 1950 The photochemistry of atmospheric water vapour *J. Geophys. Res.* **55** pp 301–327
[15] Krassovsky V I 1963 Chemistry of the upper atmosphere, in: Priester, W. (Ed), Space Research, 3, North-Holland Publ Co, Amsterdam pp 96–116
[16] Semenov A I, Shefov N N 1996 An empirical model for the variations in the hydroxyl emission *Geomagnetism and Aeronomy* **36(4)** pp 468–480
[17] Lin C L, Leu V T 1982 Temperature and thirdbody dependence of the constant for the reaction $O + O_2 + M \rightarrow O_3 + M$ *Int. J. Chem. Kinetics* **14** pp 417
[18] Nicolet M 1989 Aeronomic chemistry of ozone *Planet. Space Sci.* **37(12)** pp 1621-1652
[19] Kaufman F 1969 Neutral reactions involving H and other minor constituents *Can. J. Chem.* **47(10) pp** 1917-1926
[20] Nicolet M 1971 Aeronomic reactions of hydrogen and ozone, in: Fiocco, G. (Ed.), Mesospheric models and related experiments / Dordrecht: D.Reidel Publ. Co. pp 1-51.
[21] Langhoff S R, Werner H J, Rosmus P 1986 Theoretical transition probabilities for the OH Meinel system *J. Molecular Spectrosc.* **118(4)** pp 507–529
[22] Medvedeva I, Ratovsky K 2015 Studying atmospheric and ionospheric variabilities from long-term spectrometric and radio sounding measurements *J. Geophys. Res. Space Phys.* **120 (6)** pp 5151–5159
[23] Medvedeva I V, Ratovsky K G 2017 Comparative Analysis of Atmospheric and Ionospheric Variability by Measurements of Temperature in the Mesopause Region and Peak Electron Density NmF2 *Geomagnetism and Aeronomy* **57(2)** pp 217–228
[24] Mulligan F J, Dyrland M E, Sigernes F, Deehr C S 2009 Inferring hydroxyl layer peak heights from ground-based measurements from ground-based measurements of OH(6-2) band integrated emission rate at Longyearbyen (78°N,16°E) *Ann. Geophys.* **27** pp 4197-4205
[25] Yee J H, Crowley G, Roble R G, Skinner W R, Burrage M D, Hays P B 1997 Global simulations and observations of $O(^1S)$, $O_2(^1\Sigma)$ and OH mesospheric nightglow emissions *J. Geophys. Res.* **102(19)** pp 19 949–19 968